INVESTIGATION OF OPTIC FLOW, TIME-TO-INTERCEPT, AND PILOT WORKLOAD DURING AGGRESSIVE APPROACH TO HOVER MANEUVERS

Dr. Edward Bachelder, edward.n.bachelder@nasa.gov, SJSU/ US Army Aviation Development Directorate, Moffett Field, CA, USA; Dr. Martine Godfroy-Cooper, martine.godfroy-1@nasa.gov, SJSU/ US Army Aviation Development Directorate, Moffett Field, CA, USA; Bimal Aponso, bimal.l.aponso@nasa.gov, NASA ARC, Navigation Guidance and Control Systems, Moffett Field, CA, USA; Chris Blanken, Aviation Development Directorate-Ames, U.S. Army AMRDEC; Tom Berger, Aviation Development Directorate-Ames, U.S. Army AMRDEC.

Abstract

This work proposes a novel relationship between pilot workload and optic flow during visual approach-to-land maneuvers. A simulation experiment was conducted at NASA Ames Vertical Motion Simulator (VMS) to evaluate the workload associated with operating two candidate Army Future Vertical Lift (FVL) vehicles: a compound (coaxial-rotor and push-prop) vehicle, and a tilt-rotor vehicle. The UH-60 was included in the evaluation as a baseline reference. Sixteen experienced military pilots flew aggressive visual approaches terminating in a hover while providing Bedford workload ratings in real time. No approach or hover guidance was displayed to the pilot. The out-the-window (OTW) environment (front and chin monitors) was digitally recorded and the optical flow of each video frame computed. Prior work identified a mathematical relationship between pilot workload and the combination of display error rate and stick rate during compensatory tracking tasks. The current work extends this relationship to visual landing approaches, where the pilot is hypothesized to track key optical variables that are available from the OTW scene. Via correlation analysis a set of candidate tracking variables which appears to drive pilot workload is identified: the rate of change of optical flow, and the angle formed between the cockpit glareshield and the intended landing spot. Combined with stick rate these variables are used to generate a Bedford estimate. Actual and modeled Bedford ratings are compared for the compound aircraft (video for the other aircraft will be processed and presented in a future paper. Innovative contributions of this research include: 1) Optical flow from high resolution, high frame rate flight video is computed and analyzed for workload analysis; 2) A modelling technique is developed that produces workload estimates that closely matches actual pilot ratings; 3) A technique based on visual perceptual requirements allows optical flow to be employed in a very simplistic, tractable, yet effective manner; 4) While tau motion theory (i.e. rate of instantaneous time-to-arrive is approximately constant) was roughly observed during the approaches, it appears that tau motion was a result of the pilot adhering to a strategy of minimizing deviation in optic flow rather than being the source of pilot behavior. This preliminary, significant conclusion proceeds from the observation that workload correlated well and was causal with minimizing change in optic flow, but correlated poorly and was often non-causal with changes in tau motion; 5) Using a novel method, Bedford workload ratings were collected in real time without impinging on the flight task, enabling in-situ workload analysis. Potential applications include: a) If a pilot has transferred control to automation during an approach in an Optionally Piloted Vehicle (OPV), pilot trust may be higher if he/she observes system behavior that resembles what a skilled operator would produce, i.e., optic flow control; b) Control of optic flow may be an effective, robust method for autonomously executing power-off (autorotative) flight to the ground.

1. INTRODUCTION

The U.S. Army Future Vertical Lift (FVL) Operations Concept Team (OCT) conducted a series of tests at NASA Ames Vertical Motion Simulator (VMS) to evaluate the maneuverability and handling qualities of two candidate notional airframe concepts envisioned to support the FVL program. Taking advantage of the pool of pilots available for this test, an experiment was conducted to investigate the influence of optic flow and time-to-intercept on pilot workload during aggressive visual approaches. While the approach-to-landing task for both fixed and rotary-wing has been examined and modeled in various ways over many decades, the task and associated pilot workload had not previously been examined

Presented at 44th European Rotorcraft Forum, Delft, The Netherlands, 18-21 September, 2018

using advanced computer vision techniques such as optic flow estimation. Such an investigation has the potential to provide insight into the fundamental perception and control processes employed during the high-speed approach task.

Two candidate FVL vehicle models were employed: an aircraft with a compound coaxial rotor and pusher propeller, and a tiltrotor vehicle. The UH-60 Blackhawk was included in the evaluation as a baseline reference for the two FVL vehicles (see Figure 1). Sixteen pilots participated in the experiment, selected by the Operations Concept Team to span the U.S. military branches and a wide range of platform and mission experience. The average number of hours flown was 2,648, the minimum and maximum were 1,350 and 4,600 hours, respectively. All approaches commenced at 120 knots and 1.5 nautical miles out from the landing zone, and the objective was to establish a hover in minimum time over the landing zone (LZ) while maintaining flight safety. The approaches were initiated at two altitudes: 200 feet above ground level (AGL) (shallow approach) or 600 feet AGL (steep approach).

a.

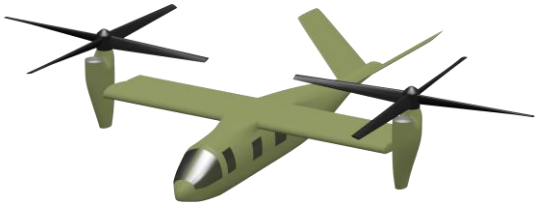

b.

c.

Figure 1. Vehicle models used in study: a) Compound; b) Tilt Rotor; c) UH-60 Blackhawk.

2. OPTIC FLOW

Optic Flow due to Translation

Optic flow is the pattern of apparent motion of objects, surfaces, and edges in a visual scene caused by the relative motion between an observer and a scene. [1,2]. Optical flow describes a sparse or dense vector field, where a displacement vector is assigned to certain pixel positions, that points to where that pixel can be found in the next image. The concept of optic flow was introduced by Gibson to describe the visual stimulus provided to animals moving through the world [3]. The application of optic flow includes the problem of inferring not only the motion of the observer and objects in the scene, but also the structure of objects and the environment. There are numerous techniques for estimating actual flow (i.e., actual motion through space) from observed optic, such as phase correlation, block-based differential, discrete optimization, which are found in the Middlebury Benchmark Dataset [4].

Differential methods belong to the most widely used techniques for optic flow computation in image sequences [5]. They can be classified into local methods such as the Lucas–Kanade technique or Bigün's structure tensor method, and global methods such as the Horn/Schunck approach and its extensions. Often local methods are more robust under noise, while global techniques, such as the Horn-Schunck Method [6], yield dense flow fields. Energy minimization, which employed by the Horn-Schunck Method, yields very accurate, dense flow fields, but can fail as displacement get too large.

Optical flow fields are useful for several navigation tasks, including landing. The rate of optical flow increases with offset from straight ahead and decreases with distance in front of the observer. The point of no optical flow has been called the “focus of expansion” (FoE) and specifies the direction of travel. For the visual landing task, much of the approach will result in low-displacement optical flow, making the Horn-Schunck Method well-suited for analysing landing video.

Barrazaa and Grzywacz [7] suggested that the human visual system is capable of decomposing complex motion patterns into basics components. Such decomposition is a property of particular theoretical and practical relevance, permitting the following assumptions simplifications.

Geometric and Effective Optic Flow

Figure 2 shows the optic flow vectors for two successive distances from LZ. The flow vectors were generated from Matlab’s Image Processing toolbox using the Horn-Schunck Method. The length and direction of the optical flow vectors

Presented at 44th European Rotorcraft Forum, Delft, The Netherlands, 18-21 September, 2018

provides an indication of the motion information available to the pilot.

The geometry for optic flow on a point on a vertical surface (Eqn. 1) and horizontal surface (Eqn. 2) generated by vehicle motion is depicted in Figure 3, where optic flow is the rate of the angle subtended by the apparent motion of a point on the ground or building. In Eqn. 2 the horizontal optic flow, $\dot{\varsigma}$ is comprised of forward velocity V_x and vertical velocity V_z, and their corresponding scaling factors. Assuming the only source of optic flow (Ω) is from $\dot{\varsigma}$, then the fraction of Ω associated with forward velocity, Ω_x, is given by Eqn. 4 (Figure 4), with the scaling factors for each velocity component given in Eqn. 3. If there was a lateral motion component (V_y) the scaling factor K_y would be identical to K_z since both axes (z and y) are approximately normal to the viewpoint. It will be shown later that the requirement for keeping the LZ in view above the cockpit glareshield (see Figure 18) ensures that line-of-sight (LOS) angle to the LZ with respect the horizontal (ς) will normally be less than fifteen degrees for all but the termination of the approach, so that a small angle approximation ($\tan\varsigma \approx \varsigma$) makes flow sensitivity in the z axis to V_z nearly the same as flow sensitivity to V_y in y axis.

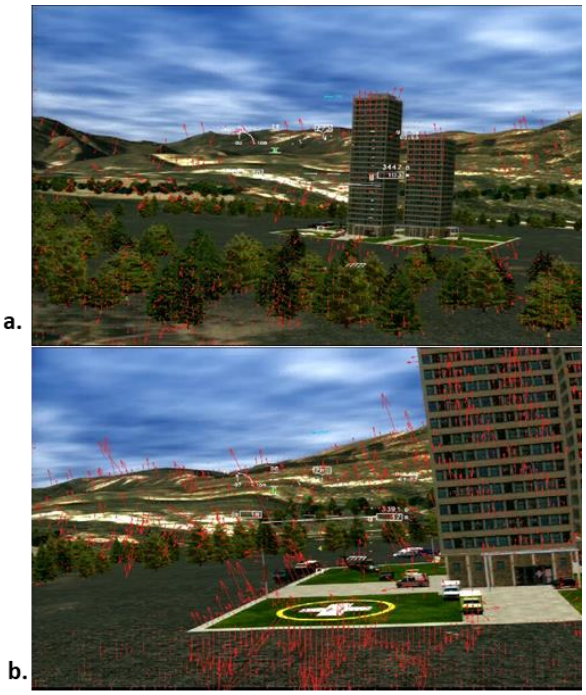

Figure 2. Optical flow (red vectors) for OTW scene for two successive distances from LZ.

(1) $\Delta\beta \approx \frac{\Delta H}{D} \Rightarrow \dot{\beta} \approx \frac{V_z}{D}$ *Optic Flow along vertical plane*

(2) $\Delta\varsigma \approx \frac{H\Delta D}{D^2} - \frac{\Delta H}{D} \Rightarrow \dot{\varsigma} \approx \frac{HV_x}{D^2} - \frac{V_z}{D}$ *Optic Flow along horizontal plane*

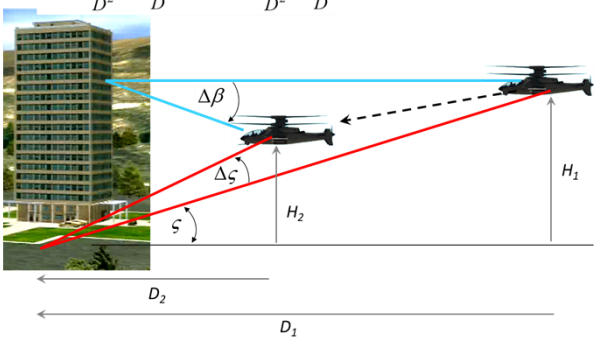

Figure 3. Geometry for optic flow on vertical and horizontal surfaces generated by vehicle motion.

Padfield [13] produced data indicating that during level flight pilots appear to extract optic flow information out to about sixteen eye-heights in front of the aircraft (i.e., the useful distance for extracting optic flow from the environment is approximately proportional to the viewer's height above ground with a factor of sixteen). Assuming this height-distance ratio in Eqn. 5, the geometrical fractions of Ω_{tot} due to V_x, V_y, and V_z are given in Eqns. 6 – 8.

(3) $$\Omega_{tot} = K_x|V_x| + K_y|V_y| + K_z|V_z| \Rightarrow K_x = \frac{H}{D^2}, \quad K_y = K_z = \frac{1}{D}$$

(4) $$\frac{\Omega_x}{\Omega_{tot}} = \frac{K_x|V_x|}{K_x|V_x| + K_y|V_y| + K_z|V_z|} = \frac{|V_x|}{|V_x| + (K_z/K_x)(|V_y| + |V_z|)}$$

(5) $$\frac{K_z}{K_x} = 16 \text{ if } D \approx 16H$$

(6) $$\frac{\Omega_x}{\Omega_{tot}} = \frac{|V_x|}{|V_x| + 16(|V_y| + |V_z|)}$$

(7) $$\frac{\Omega_y}{\Omega_{tot}} = \frac{|V_y|}{(1/16)|V_x| + |V_y| + |V_z|}$$

(8) $$\frac{\Omega_z}{\Omega_{tot}} = \frac{|V_z|}{(1/16)|V_x| + |V_y| + |V_z|}$$

Figure 4. Relationships between geometric optic flow, velocity, and observer position relative to a point located sixteen eye-heights ahead.

Assuming there is sufficient optic flow to perceive the translational rates of the three axes, it is hypothesized that an observer can decouple motion such that the magnitudes of V_x, V_y and V_z relative to one another are perceived. For this to occur the observer would effectively apply the inverse of each of the scaling factors K to the geometrical perception of each component of optic flow. This is not an unreasonable hypothesis since pilots must judge relative rate of closure in the three dimensions during a visual landing. Eqns 9 - 12 in

Presented at 44th European Rotorcraft Forum, Delft, The Netherlands, 18-21 September, 2018

Figure 5 give the effective ratios of the total optic flow that the pilot might employ to control a vehicle's motion in space. The geometrical relationships in Figure 4 are composed of denominators that are linear combinations of V_x, V_y, and V_z. It will later be shown that the simple addition of the three orthogonal velocities better represents the observed data than using the resultant of them. Applying a cognitive scalar to each optic flow component should be an intuitive element of the task for a skilled pilot. Reiterating, precise inversion of each scalar *K* in Figure 4 would not be necessary – an inversion based on scalars that are proportional to one another would suffice. For instance, say K_x = 2, K_y = 3, and K_z = 4. If the vector 0.8*{1/2 1/3 1/4} was applied to the *K*'s of the denominators and numerators instead of the precise vector {1/2 1/3 1/4}, the result would be the same.

$$\Omega_{tot} = K_x|V_x| + K_y|V_y| + K_z|V_z| \quad (9)$$

$$\frac{\Omega_x^{eff}}{\Omega_{tot}} = \frac{|V_x|}{|V_x| + |V_y| + |V_z|} \quad (10)$$

$$\frac{\Omega_y^{eff}}{\Omega_{tot}} = \frac{|V_y|}{|V_x| + |V_y| + |V_z|} \quad (11)$$

$$\frac{\Omega_z^{eff}}{\Omega_{tot}} = \frac{|V_z|}{|V_x| + |V_y| + |V_z|} \quad (12)$$

Figure 5. Relationships between effective optic flow and velocity.

It is not possible for all the states of self-motion (heading, rate of turn, impact point, etc.) to be obtained using the optic flow arising from just one point or a line of points [8] located on the ground, rather perception of self-motion generally makes use of the optic flow field where it is available in the scene and where it is most informative. Optic flow density will vary in time with texture and scene structure changes, requiring the viewer to dynamically focus or expand areas of interest in the scene.

Using the equations in Figure 5 and the recorded aircraft speeds, the effective fraction of the sum of total optic flow used to conrol V_x, V_y and V_z are shown in Figure 6 for one of the tested runs (it is assumed that rotational speeds are zero).

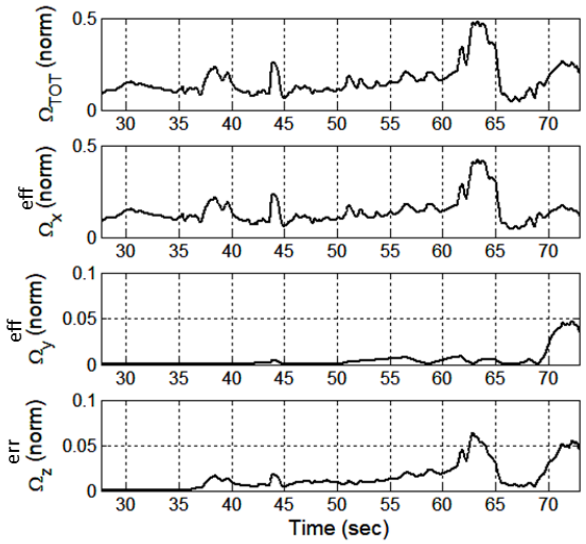

Figure 6. Normalized effective optical flow (sum of magnitudes): a) Total; b) Forward axis; c) Lateral axis; d) Vertical axis (note the different scale in c and d).

Optic Flow due to Changing Terrain Height and Aircraft Rotation

In the previous section it was assumed that the aircraft was not rotating (i.e., yaw, pitch and roll rates were zero). Figure 7 examines optic flow arising from angular motion of the aircraft, assuming a field-of-view (FOV) < 50 degrees in both the vertical and horizontal, and $|\phi|$ (roll angle) < 15 degrees. Pitch motion translates vertically all pixels in the scene equally at the same rate as pitch (Eqn. 13), and similarly yaw motion translates horizontally all pixels in the scene equally at the same rate as yaw (Eqn. 14). Roll produces optic flow normal to each pixel's radius from the center of rotation, and proportional to the radius length. For pixels located at the extremities of the globe relative to the viewer's LOS (i.e., μ = +/- 90 degrees, see wireframe globe in Figure 7), the optic flow is at a maximum and equal to the roll rate itself. At the center of rotation the optic flow due to roll rate is zero. Since optic flow due to $\dot{\phi}$ varies with the sine of its angular location in the image (μ and λ), then for a scene FOV < 50 (actual FOV of the recorded OTW scene in the experiment was 48Hx36V degrees) in both the horizontal and vertical the contribution of $\dot{\phi}$ to optic flow would be negligible. Thus optic flow due to aircraft rotation would principally be due to $\dot{\theta}$ and $\dot{\psi}$.

Presented at 44th European Rotorcraft Forum, Delft, The Netherlands, 18-21 September, 2018

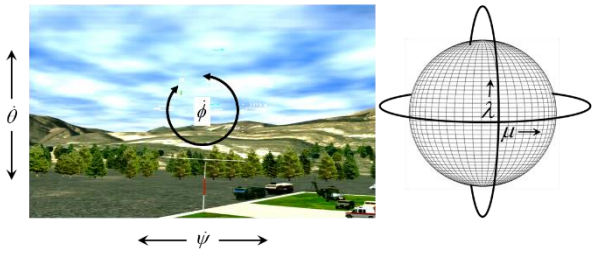

For narrow FOV (< 50 *deg hor/ver*)

(13) Pitch (θ) translates all pixels by same amount vertically $\left|\Omega_i^{\theta}\right| = \dot{\theta}$

(14) Yaw (Ψ) translates all pixels by same amount laterally $\left|\Omega_i^{\psi}\right| = \dot{\psi}$

(15) Roll (ϕ) translates all pixels normal to their radius from the center of rotation $\left|\Omega_i^{\phi}\right| = \dot{\phi}\sqrt{\sin^2\lambda_i + \sin^2\mu_i} \approx \dot{\phi}\sqrt{\lambda_i^2 + \mu_i^2}$

(16) $\Omega^{rot} \approx (\dot{\theta} + \dot{\psi})$

(17) $\Omega^{tot} \approx \Omega^{trans} + (\dot{\theta} + \dot{\psi})$

Figure 7. Approximate relationships between aircraft rotation and optic flow.

Figure 8a shows the aircraft trajectory in blue and the height of the terrain in black (both are relative to mean sea level, MSL). The terrain rises and falls twice before assuming a constant height until the LZ is reached. The image FOV is 38 degrees in the vertical, the pixels that are viewable from the cockpit correspond to those forward of the aircraft and within the blue-shaded region of Figure 8a. Prior to about the 8-second mark the relative height of all the viewed terrain is increasing, reaching a maximum at 8 seconds. This in turn increases the optic flow even though the aircraft remains at constant MSL altitude and constant speed. After 8 seconds more of the distant terrain comes into view, so that optic flow would in general decrease as the final terrain peak is approached and crossed. As noted earlier, scene content will affect the texture from which optic flow is computed, and areas that are texture-poor will serve to reduce overall optic flow, and the converse is also true (hence the slight variations in optic flow when the FOV has cleared the final peak). The pilots almost always commenced the approach when over the level stretch of terrain, so that optic flow computed during the approach did not vary due to terrain height.

Pitch rate for the example shown in Figure 8 peaked at the 43-second mark. If all the pixels in the image scene had sufficient texture, then each pixel would have been translated in the vertical at the same rate at pitch – superimposed on this would have been the optic flow components due to aircraft translation and yaw and roll rotation. However, many scene pixels lacked texture (i.e. the sky, clearings between trees), and did not register much if any optic flow. The number of pixels in the scene that were 'active' (i.e., registered) were identified, assigned the pitch and yaw rates as optic flow, summed, divided by the total number of pixels in the image (1024x768), and converted to milliradians/sec. This is shown in red in Figure 8b and represents the average optic flow due to aircraft rotation only. Much of the high-frequency content of the optic flow is due to rotation, but in general this is low-amplitude relative to the contribution due to translation except for momentary periods. As a first approximation the assumption of zero optical flow due to rotation (for the approach maneuver) is generally valid.

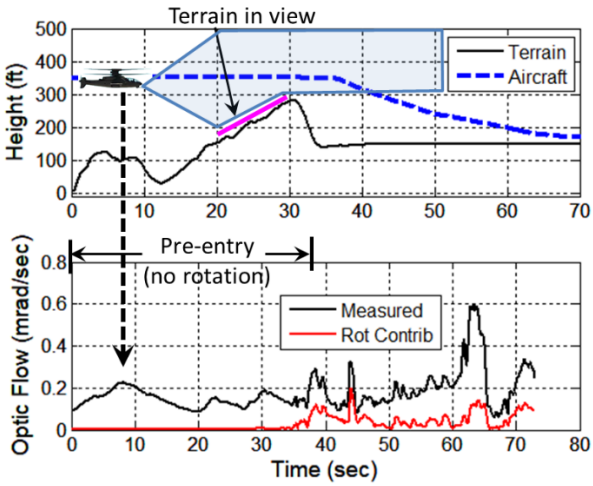

Figure 8. Effects of terrain height and aircraft rotation on optical flow: a) Terrain height and aircraft altitude relative to starting time; b) Global optic flow (black) and optic flow due to aircraft rotation (red).

Optic Flow and Helicopter Manoeuvres

Loomis and Ball [9] examined various visually controlled manoeuvres in the 'spirit of similar analyses by Gibson, and Turvey and Remez'. One category of these tasks was Regulation of Braking, Docking, and Vertical Landing, and the following two approaches were offered as candidate guidance strategies. In 1976 Lee [10] proposed a theory of braking based on the optical variable, tau (τ), which is the ratio of the angular extent of the object ahead divided by its time derivative, the rate of optical expansion. Thus τ represents instantaneous time-to-arrive. The optimal control strategy is to decelerate in such a way as to maintain the derivative of τ at a value greater than or equal to -0.5. Yilmaz and Warren [11] provided support for the theory by showing that operators employed a strategy close to the optimal one and that manipulating the availability of distance cues had little effect on performance. However, Flach, Stanard, and Smith [12] provided data and an analysis suggesting that operators regulate their stopping behaviour using the optical expansion rate itself.

Presented at 44th European Rotorcraft Forum, Delft, The Netherlands, 18-21 September, 2018

Padfield [13] showed that pilots conducting various flight manoeuvres in proximity to the terrain produced behaviour consistent with tau motion theory.

Quoting a prior Army helicopter instructor, “Army instructor pilots teach students and evaluate rated pilots on the technique that a normal approach should have the appearance of a fast walk from approach to land entry to just before touch down. This is to ensure a steady and continuous deceleration of the aircraft to arrive at the intended touchdown point with zero airspeed.” This would imply that the strategy is to maintain the observed optic flow constant following approach entry. As will be seen in the results of the current work, both the tau motion and optical expansion hypotheses may be consistent in describing how helicopter pilots conduct aggressive landing approaches.

3. WORKLOAD MODEL DEVELOPMENT

The earliest study of the human operator as a linear servomechanism is that of Tustin [14] who proposed that, despite amplitude nonlinearities, temporal discontinuities and haphazard fluctuations, there might be an “appropriate linear law” that would describe the main part of the operator’s behavior. Insight from servomechanical design led McRuer [15] to develop the ubiquitous human crossover model (*CM*), which within its framework accounts for how, and why, the human operator adapts to the controlled plant dynamics during compensatory tracking. With the *CM*, a variable pilot time delay can be used to explain phenomena such as increased high-frequency phase lag associated with increased amounts of error lead equalization.

Bachelder [16] extended Hess’ Structural Model [17,18] to account for and reproduce pilot compensatory behavior when different control styles are used. It is shown that the pilot’s internal prioritization (or costing) can be approximated as simply the product of workload (relative to remaining spare capacity) and performance (how well the pilot nulls the displayed error signal). For two very different compensatory tracking tasks (one was single-axis, the other four-axis tracking), Bachelder [19] demonstrated that pilot workload can be estimated as the product of the standard deviation of filtered stick rate and error rate raised to a power *k*, shown in Eqn. 18.

$$B_{est} = b*(\sigma_{\dot{\delta}_f}\sigma_{\dot{e}_f})^k + c \quad (18)$$

where B_{est} is the estimated Bedford workload rating (described in a later section), and the elements *b* and *c* are task-specific constants. The current work intended to extend this relationship to visual landing approaches, where the pilot is hypothesized to track key variables that are available from the OTW scene.

Lu et al. [20] conducted an experiment using single-axis lateral-reposition task whose display and controller are represented in Figure 9. The time-weighted total compensatory effort (TWTCE) performance metric [21] was cited as a potential measure of workload, whereby an idealized control input based on a tau template (without the addition of any stabilization activity) is compared to the actual control output.

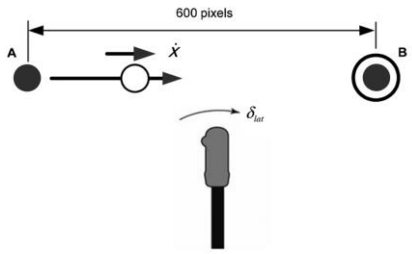

Figure 9. Schematic of single-axis lateral-reposition pilot task conducted by Lu et al. [20].

A method similar to this was initially explored whereby it was hypothesized the pilot created an internal tau template for the forward speed at the start of the landing approach, and modulated vertical speed as required to maintain a constant glideslope to the LZ. However, virtually all pilots were observed to produce multiple minima in sink rate, and often in forward speed (Figure 10), grossly

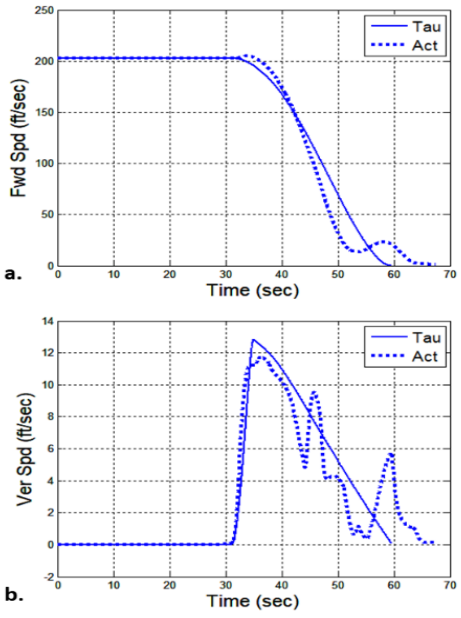

Figure 10. Example comparison of predicted tau motion and actual motion for one pilot (Coaxial aircraft, shallow appproach): a) Forward speed; b) Vertical Speed.

Presented at 44th European Rotorcraft Forum, Delft, The Netherlands, 18-21 September, 2018

inconsistent with any initial tau template. Resetting the template when minima were encountered did not correlate well with the workload ratings.

A potentially complicating factor is the manner in how forward speed is controlled with the coaxial aircraft. Pilots could manually command positive and negative propeller thrust using a spring-centering fore/aft thumb lever, or could choose to use buttons that drove the thrust to pre-set values (50%, 0%, -50%). The thrust increased/decreased at a constant rate of 8% per second. Speed response during thrust transition was very rapid and nonlinear, making difficult to anticipate. Additionally, the cost of overshoot (losing sight of the LZ, over-compensating afterwards with reverse thrust) was greater than undershoot, so pilots tended to decelerate conservatively and resume building forward acceleration when the approach became excessively slow. Figure 11 gives altitude, forward and vertical speed time histories for the associated maneuver. Since the objective was to hover over the LZ at 10 feet in minimum time, pilots maintained initial speed and altitude for as long as possible after simulation release before commencing descent and slowdown.

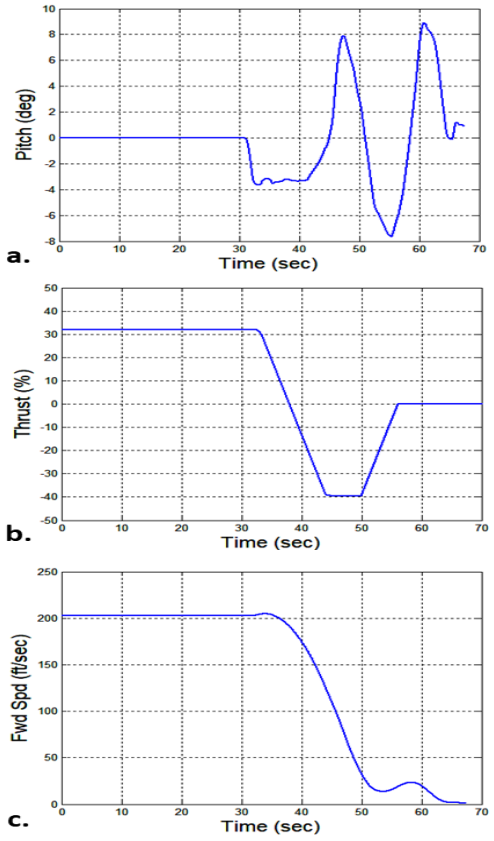

Figure 11. Histories of aircraft states affecting down-range distance response (Coaxial aircraft, shallow approach, one pilot): a) Pitch; b) Propeller thrust; c) Forward speed.

Seeking to identify the analog to the tracking error that was employed in compensatory tracking (Eqn. 18), it was observed that changes in workload appeared to be accompanied by changes in the measured optic flow Ω. It will be shown in the Results section that in addition to the pilots also appeared to be tracking $\dot{\Omega}$ during the approach.

4. FLIGHT SIMULATION EXPERIMENT

4.1.1 Vehicle Models

Three aircraft models were flown: two candidate FVL vehicles (a compound aircraft with a coaxial rotor and pusher propeller, and a tiltrotor vehicle), and the UH-60 Blackhawk. The flight dynamics models of the lift offset coaxial-pusher and tiltrotor configurations were developed using the U.S. Army Aviation Development Directorate (ADD) in-house flight-dynamics modeling software tool-HeliUM [22,23]. HeliUM uses a finite-element approach to model flexible rotor blades with coupled non-linear flap/lag/torsion dynamics to capture structural, inertial, and aerodynamic loads along each blade segment, a key requirement for these advanced rotorcraft configurations. Blade, wing, and fuselage aerodynamics come from non-linear lookup tables, and the rotor airwakes are modeled using a dynamic inflow model. A multi-body like modeling approach is used to build the aircraft configuration from its independent components (e.g., fuselage, wing, nacelle, etc.), which allows modeling of arbitrary aircraft configuration with multiple rotors.

The models are generic and are not meant to represent specifically the industry designs. The coaxial-pusher configuration was derived from a previous rotorcraft sizing trade-off study [24], which gives the overall dimensional and weight characteristics as well as key rotor and aircraft aerodynamic properties. The generic tiltrotor configuration was derived from scaling geometric, inertial, and structural properties of the XV-15, V-22, and the notional NASA Large Civilian Tilt-Rotor 2 (LCTR2). Berger et al. [25] presents a detailed description of the coaxial-pusher and tiltrotor models.

The UH-60 Black Hawk model employed is a non-linear blade-element model, based on the Sikorsky General Helicopter (GenHel) Flight Dynamics Simulation. GenHel is a total force, large angle model, including six rigid body degrees of freedom, as well as rotor blade flapping, lagging and hub rotational degrees of freedom. The UH-60 Primary Flight Control System (PFCS) is comprised of a Stability Augmentation System (SAS) and a Flight Path Stabilization (FPS) system, as well as sensor and mechanical system models. The SAS is ten percent, limited authority (five percent digital plus

Presented at 44th European Rotorcraft Forum, Delft, The Netherlands, 18-21 September, 2018

five percent analog) for pitch, roll and yaw. The FPS is a full-authority, rate-limited feedback system for the lateral, longitudinal and yaw axes, which was designed to ease pilot workload. It works by generating a trim signal that back-drives the cyclic and pedals.

4.1.2 The Simulation Facility

The experiment was performed in the Vertical Motion Simulation (VMS) complex at NASA Ames Research Center. The simulator was fixed-base (no motion) with LCD displays providing the OTW scene and view through the chin-bubble (see Figure 12). Numerical data (vehicle state, control inputs, etc.) were recorded at 100 Hz, and video was recorded at 30 Hz. The OTW video resolution was 1024x768, and chin-bubble video resolution was 768x1024.

Figure 12. View of simulator cockpit showing chin-bubble display.

R-Cab

The experiment was conducted in the ICAB area as a fixed-base experiment using R-Cab, the cab designed for rotorcraft operations. The cab was configured with a single seat on its centreline equipped with rudder pedals, a cyclic, a power control lever serving as collective, and a sidestick. The cyclic was used when flying the UH-60 model and the sidestick used for the coaxial and tilt-rotor. All inceptors were hydraulically actuated.

View of the OTW scene was provided by a display to the pilot's left, one straight ahead and one to the right. Additionally, a flat-screen monitor was placed to the pilot's lower right to approximate to the view from a chin window.

Representative aircraft sounds, (engine, rotor and aero noises among others), were played in the cockpit. Headsets permitted two-way communication with the control room over an open mic. A cockpit camera permitted Control Room monitoring of the cockpit and pilot.

4.1.3 Experimental Protocol

Pilots conducted visual approaches to the same LZ commencing at 120 knots and 1.5 nautical miles out (see Figure 13), with the objective of safely establishing a hover in minimum time over the LZ. The approaches were initiated at one of two altitudes, 200 feet AGL (shallow approach) or 600 feet AGL (steep approach) shown in Figure 14. The first eight pilots were instructed to complete each approach in minimum time while maintaining flight safety. The second eight pilots were told that a primary objective was to 'beat the clock'- for a given aircraft and altitude condition they would attempt to complete each approach in less time than the previous approaches within that condition. Elapsed time after simulation release was displayed on the head up display (HUD). The intent for creating the two groups was to generate a greater spread of performance and workload across pilots to more effectively identify cause and effect.

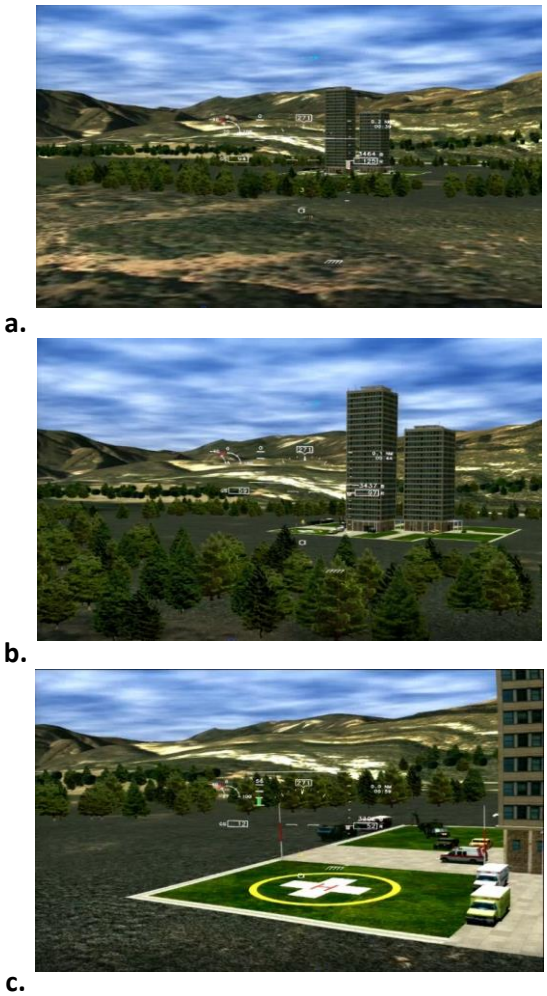

a.

b.

c.

Figure 13. Out-the-window view during the approach for diferent distances from the LZ: a) 1,200 feet; b) 600 feet; c) 200 feet.

Presented at 44th European Rotorcraft Forum, Delft, The Netherlands, 18-21 September, 2018

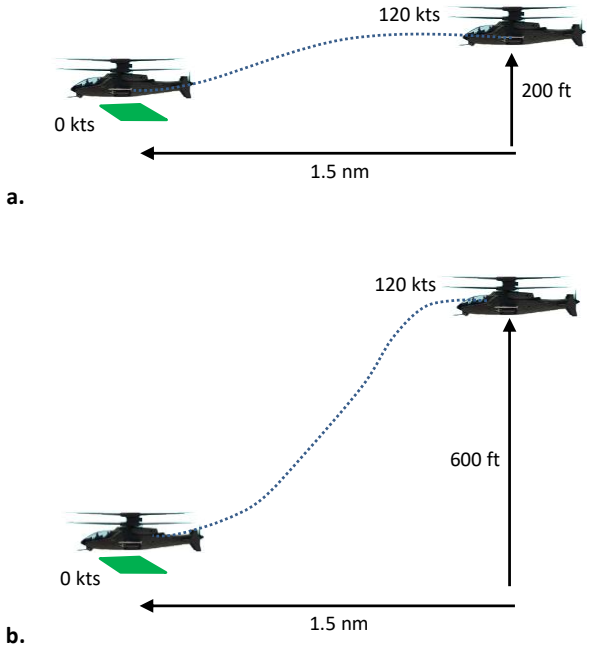

Figure 14. Approach profiles: a) Shallow approach (200 feet); b) Steep approach (600 feet).

The pilots obtained visual flight cues from OTW environment, and basic aircraft states on the HUD, as seen in Figure 15b. (flight path marker was not provided). The pilots were instructed to use a Bedford rating scale (Ref. 2) to provide an estimate of their workload during the approaches. Pilots verbally reported the Bedford rating when it was perceived as having changed from the last update. The verbalized Bedford was displayed at the bottom of the HUD (Figure 15b). An example time history of pilot Bedford rating is shown in Figure 15a. The video frame in Figure 15b was captured 20 seconds into the maneuver, and the Bedford rating of 2 associated with this time is indicated on the right by a red star. Note that workload has begun to increment prior to the pilot initiating control movement at 31 seconds.

When the pilot felt he had established in a steady 10 foot hover over the LZ he would make the announcement “arrived”. After 10 seconds of hover the instruction was given to either perform a left or right pedal turn for 180 degrees, then land.

4.1.4 Participants

Sixteen male U.S. military pilots, aged 32 to 46 (average age 37.5) participated in the experiment. Mean flight time was 2793 flight hours (standard deviation (STD) was 1277). Nine of the pilots were Army, three Marine Corps, two Air Force, and two Coast Guard. One had a fixed-wing background which included flying the V-22 Osprey, the remaining had flown rotary-wing in their military assignments.

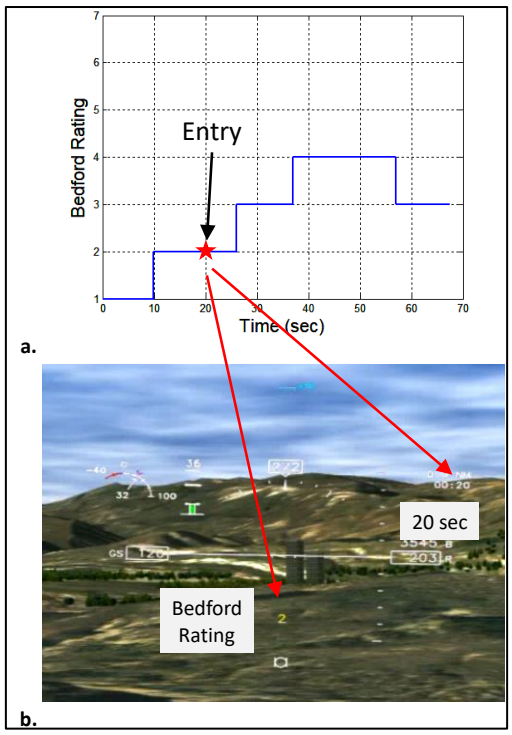

Figure 15. a) HUD showing Bedford rating 20 seconds into maneuver (Coaxial aircraft); b) Pilot Bedford rating time history for entire maneuver (approach was entered at 31 seconds).

4.1.5 Imagery, Display, and Recording

The location of the scene was Wheeler Springs in Ojai, California. The visual system uses Rockwell-Collins computer-generated imagery (CGI) with aerial and satellite imagery. Figure 16 gives the FOV for each of the cockpit displays. The central display FOV was 48x36 degrees, which was the display recorded and analyzed for optic flow. The graphical FOV was conformal with the physical FOV, so that there was no virtual compression of the imagery which otherwise would have affect optical flow. Video imagery of the CGI was recorded at a rate of 30 Hz with a resolution of 1024x768. Aircraft state and pilot control position data was collected at 100 Hz. The Digital Elevation Model resolution was one meter.

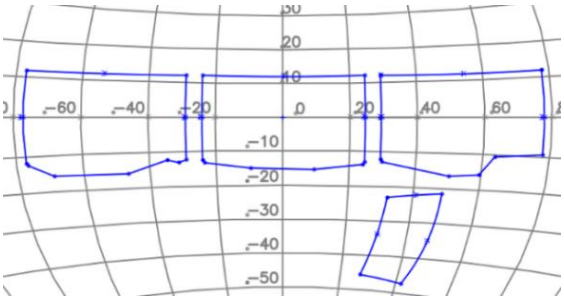

Figure 16. Field-of-View map for R-Cab cockpit displays.

Presented at 44th European Rotorcraft Forum, Delft, The Netherlands, 18-21 September, 2018

4.1.6 Experimental Design

Each pilot flew a total of 18 runs, with altitude and aircraft type as condition variables (both variables were counterbalanced between pilots). For each vehicle type pilots flew both altitudes before flying another aircraft. Table 1 shows the design matrix.

Table 1. Experimental Design

Aircraft	Start Altitude (ft)	Trials
Blackhawk	200	3
	600	3
Compound	200	3
	600	3
Tilt Rotor	200	3
	600	3

4.1.7 Training

Prior to flight training the Bedford rating scale was explained to pilots and the rating flow chart given to pilots to study. Pilots then trained on a given aircraft when that aircraft was next in the experimental matrix. For instance, if the vehicle order to be flown was Tilt Rotor, Coaxial and Blackhawk, pilots would first train with the Tilt Rotor, conduct runs for data collection with that aircraft, and then proceed to train with the Coaxial vehicle. Within a vehicle type the training was as follows. At 200 feet two runs were flown at constant altitude, with the objective of arriving abreast of the tower adjacent to the LZ (Figure 13) in minimum time and with zero airspeed and vertical descent. This was followed by two full approaches conducted at 200 feet, and two full approaches initiated at 600 feet. The altitude order that the pilots flew for data recording was counterbalanced across pilots and vehicle types.

4.1.8 Measures of Performance and Workload

Objective data

Measures of performance are given and defined in Table 2. Figure 17 depicts the geometries relevant to the approach task, with the angle between the cockpit glareshield (see Figure 18) and the LZ (termed LOS reference angle, η) being particularly important. The glareshield edge is located approximately fifteen degrees below the aircraft body axis, depending on actual eye-height of the pilot.

Table 2. Measures of performance. Std= standard deviation.

Measure		Description
t_comp		approach completion time
perc_x		% of maneuver for which τ_x < 20 sec (x-axis)
perc_z		% of maneuver for which τ_z < 20 sec (z-axis)
perc_diff		% of maneuver for which $\lvert\tau_x - \tau_z\rvert$ < 20 sec
los_diff_std	$\sigma(\eta)$	std of angle between LOS and glareshield
los_diff_dot_std	$\sigma(\dot{\eta})$	std of d(angle between LOS and glareshield)/dt
los_ang_std	$\sigma(\varsigma)$	std of LOS angle
los_ang_dot_std	$\sigma(\dot{\varsigma})$	std of d(LOS angle)/dt
lon_rate_std		std of longitudinal stick rate
lat_rate_std		std of lateral stick rate
col_rate_std		std of collective rate
fpa_std	$\sigma(\gamma)$	std of flight path angle
fpa_dot_std	$\sigma(\dot{\gamma})$	std of d(flight path angle)dt
theta_std	$\sigma(\theta)$	std of pitch
q_std	$\sigma(\dot{\theta})$	std of pitch rate

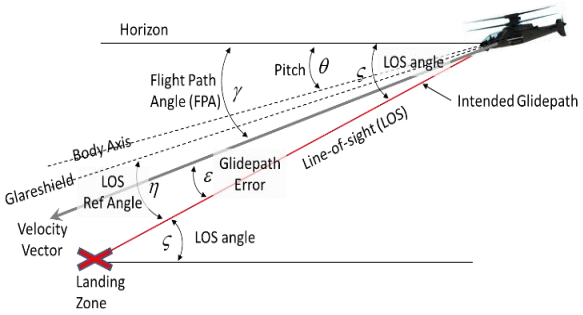

Figure 17. Variables corresponding to geometry of approach-to-landing.

Figure 18. Simulator cockpit glareshield.

Figure 19a shows the time-to-arrive (tau) for the forward (*x*) and vertical (*z*) axes for an approach using the Coaxial aircraft. There are minor oscillations in τ_x, but much larger ones in τ_z. If a constant glidepath angle were flown, both tau histories would be identical. In Table 2 the measures *perc_x* and *perc_z* is the percentage of

Presented at 44th European Rotorcraft Forum, Delft, The Netherlands, 18-21 September, 2018

the time after entry that τ_x and τ_z are less than 20 seconds, respectively. *perc_diff* is the percentage of time that the difference between τ_x and τ_z is less than 20 seconds.

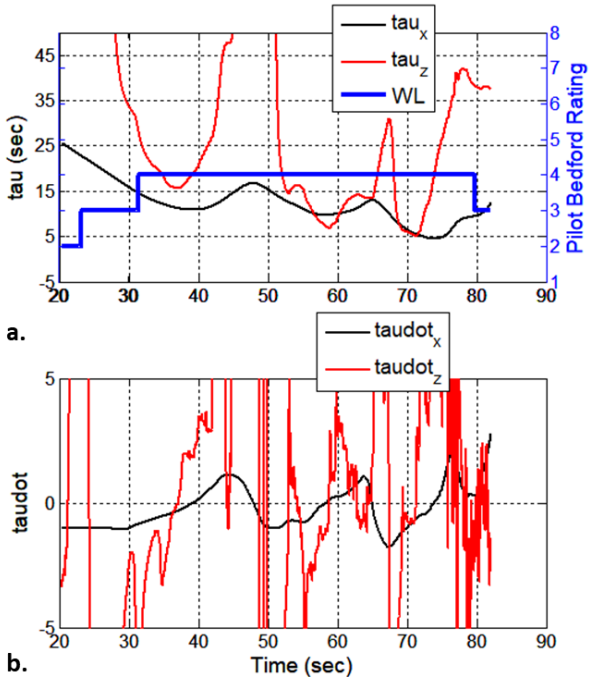

Figure 19. Tau behavior during an approach: a) τ_x, τ_z, and pilot bedford rating; b) $\dot{\tau}_x$ and $\dot{\tau}_z$. Tau z data have been clipped to show the variations of tau x and WL.

Subjective data:

Bedford ratings were collected as described in Experimental Protocol, and at the end of each vehicle type run, pilots provided verbal comments which were recorded in audio files.

5. RESULTS

5.1.1 Workload Model and Optic Flow

Analyses related to optic flow was conducted only with the coaxial aircraft data in this current work, optic flow computed from the recorded video for the other aircraft will be examined in the future. Thus Section 5.1.2 pertains only to the coaxial vehicle. Six of the pilots had used the Bedford rating scale previous to the experiment, and nine had not. Examining the workload scores for the coaxial aircraft, Table 3 shows that on average both the maximum Bedford rating (B_{max}) and the average rating (B_{avg}) more than doubled when pilots had previous exposure. Of the ten pilots who did not have prior Bedford experience, three of them gave ratings of '1' for the entire duration of each flight when using the coaxial aircraft. For brevity and levity this group will be called the Flatliners.

Table 3. Bedford ratings for pilots who did and did not have previous experience using the Bedford scale.

Experience Using Bedford?	Yes (N = 6)	No (N = 10)
Mean(B_{max})	5.3	2.5
Mean(B_{avg})	3.9	1.9

Because of the large difference in workload response between the two groups shown in Table 3, workload modelling for the visual approaches was developed using the group that possessed prior experience with Bedford rating.

Variable Correlation with Workload

It is tempting but often difficult to positively attribute correlation to causality. Low correlation, however, is a good indicator of non-causality. Within a set of variables that correlate with workload, there may be none, one, or more that actually play a part in driving workload. In a previous study Bachelder [16] gave preliminary evidence that what the pilot attempts to minimize when conducting a compensatory tracking task is approximately the product of workload and performance. The primary source(s) of workload, in conjunction with what the pilot perceives as the performance objective, should therefore constitute what drives pilot control. One method for inferring what the pilot uses for control is to establish what the minimal necessary cues are to accomplish the task. Humans, as with many phenomena found in the natural environment, are very good at producing minimalist strategies for manifold perception-control tasks.

The first variable examined for correspondence with workload was optic flow, Ω. Employing the Power Law that was used in Eqn. 18, the correlation between Ω and workload was highest when Eqn. 19 was used.

$$B_{est} = b*(\sigma_{\Omega})^{0.15} + c \tag{19}$$

The relationship between the Power Law and the perception of workload is examined by Bachelder and Godfroy-Cooper [26], where for a small exponent the Power Law approximately reduces to Weber's Law. Weber's Law states that the strength of perception is proportional to the log of the stimulus. The results of the previous work in [19] suggest that workload perception is consistent with and based on psychophysics principals To investigate the hypothesis that the pilot uses optic

Presented at 44th European Rotorcraft Forum, Delft, The Netherlands, 18-21 September, 2018

flow in a way that scales the *xyz* velocities in an *effective* manner (described earlier in Optic Flow section) rather than using the geometric appearance of optic flow for control, Table 4 compares the linear fit between Eqn. 19 and actual workload using the two methods. The vertical (z) axis shows the *effective* method to have greatest advantage over the geometric approach (i.e. it sides more with reality), followed by the longitudinal (x) axis.

Table 4. Comparison of fit (correlation coefficients) with workload using effective and geometric method to compute fraction of Ω_{tot}.

Method for Computing Fraction of Ω_{tot}	Fit (x)	Fit (y)	Fit (z)
Effective	0.79	0.83	0.87
Geometrical	0.75	0.83	0.82

The second variable examined for correspondence with workload was pilot control input using the form of Eqn. 19.

Collective rate produced the highest correlation compared to the lateral and longitudinal stick rates. Figure 20 shows the very good fit between estimated and actual Bedford using collective rate. The black dots denote mean, red bars denote standard deviation, and the size of the black dots indicate relative percentage of total measurements that comprise the mean (i.e. relative frequency that the particular Bedford rating was assigned by the pilot compared to all the Bedford ratings collected over time). Thus collective is an excellent indicator of workload, but it may not necessarily be the primary source of workload.

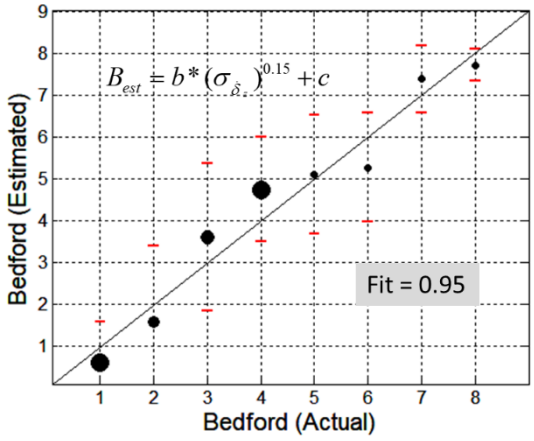

Figure 20. Bedford estimate comparison using collective rate. Black dots denote average, red bars denote standard deviation, radius of black dots denotes relative percentage of total measurements that comprise the average.

Table 5 gives the fit (correlation coefficient), average error, and standard deviation of the error for the Bedford estimate using collective, lateral stick and longitudinal stick rate. Note that the Bedford scale is ordinal.

Table 5. Stick control rate correlation with workload (fit, mean Bedford error, and standard deviation Bedford error).

Variable	Fit	Avg(B_{err})	std(B_{err})
$\dot{\delta}_z$ *collective rate*	0.95	0.45	1.09
$\dot{\delta}_y$ *lat stick rate*	0.79	1.03	1.60
$\dot{\delta}_x$ *lon stick rate*	0.78	1.07	1.63

Table 6 shows the correlation of approach variables with workload in descending order, as well as the average error and standard deviation. Collective rate ranked highest, thus this would be the best single-variable indicator of workload for the Coaxial aircraft conducting the high-speed approach task. Whether collective rate partly drives workload, is an outcome of it, or a combination of both is difficult to ascertain. The effective fraction of total optic flow supporting the longitudinal and vertical axes, Ω_x^{eff} and Ω_z^{eff}, are computed using Eqns. 10 and 12 (optic flow rate, $\dot{\Omega}^{eff}$, is computed using acceleration instead of velocity). For economy the superscript *eff* will be dropped, i.e., Ω_z used in place of Ω_z^{eff}. Note that the fit for $\dot{\Omega}_z$ with workload is 12% higher than for $\dot{\Omega}_x$.

Table 6. Correlation of approach variables with workload (fit, mean Bedford error, and standard deviation Bedford error).

Variable	Fit	Avg(B_{err})	std(B_{err})
$\dot{\delta}_z$ *stick rate*	0.95	0.45	1.09
$\dot{\gamma}$ *FPA rate*	0.92	0.60	1.28
$\dot{\varepsilon}$ *GS error rate*	0.91	0.61	1.30
γ *FPA*	0.89	0.72	1.44
$\dot{\Omega}_z$ *optic flow rate, z*	0.87	0.80	1.40
ε *GS error*	0.87	0.82	1.51
Ω_z *optic flow, z*	0.86	0.82	1.45
$\dot{\eta}$ *ref angle rate*	0.85	0.86	1.45
η *ref angle*	0.85	0.88	1.45
$\dot{\varsigma}$ *LOS angle rate*	0.85	0.83	1.55
ς *LOS angle*	0.83	0.83	1.55
$\dot{\Omega}_x$ *optic flow rate, x*	0.76	1.14	1.72
$\dot{\tau}_x$ *tau rate x*	0.62	1.79	2.63
$\dot{\tau}_z$ *tau rate z*	0.56	1.95	4.10

Presented at 44th European Rotorcraft Forum, Delft, The Netherlands, 18-21 September, 2018

Table 7 gives the fit, mean Bedford error, and standard deviation of the error for Bedford estimates using variables from Table 6 that were both observable and ranked high. Since the simulator HUD did not have a flight path marker (this was omitted by design to force the pilot to interpret and rely on OTW visual cues), it was not possible to have precise flight path or glideslope error information. Instead, what the pilot could use as a surrogate for both was the angular difference between the LZ and the cockpit glareshield (reference angle, η). Thus Ω_z, η, and their rates present themselves as candidate variables that the pilot may directly track during much of the approach.

Table 7. Correlation of approach variable combinations with workload (fit, mean Bedford error, and standard deviation Bedford error).

Variables	Fit	Avg(B_{err})	std(B_{err})
$\Omega_z\dot{\Omega}_z\eta$	0.96	0.40	1.13
$\Omega_z\dot{\Omega}_z$	0.95	0.45	1.25
$\Omega_z\eta$	0.94	0.51	1.24
$\dot{\Omega}_z\dot{\eta}$	0.93	0.55	1.14
$\dot{\Omega}_z\eta$	0.93	0.58	1.17
$\Omega_z\dot{\eta}$	0.93	0.53	1.22

The combination of Ω_z, $\dot{\Omega}_z$ and η used in Eqn. 19 (the form of the model given by Eqn. 2) gave the best fit – slightly better than collective rate used by itself in Table 5. Figure 21 shows the resulting fit.

(19) $$B_{est} = b*(\sigma_{\Omega_z}\sigma_{\dot{\Omega}_z}\sigma_{\eta})^{0.15} + c$$

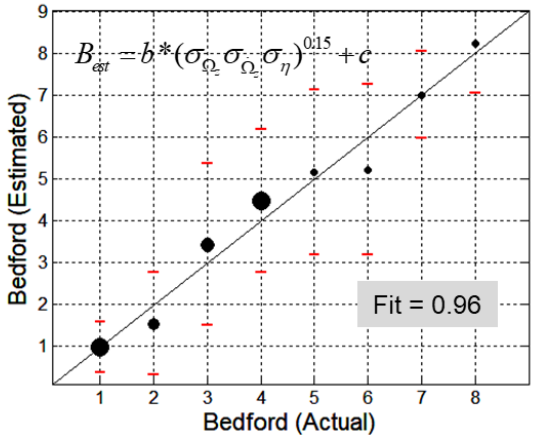

Figure 21. Bedford estimate comparison using $\Omega\dot{\Omega}\eta$ for the six pilots with prior exposure to Bedford scale who were used to construct the workload model. Black dots denote mean, red bars denote standard deviation, radius of black dots denotes relative percentage of total measurements that comprise the average.

As noted earlier, the workload model for the visual approach task was constructed using the six pilots who had previous experience with Bedford ratings. Figure 22 applies that same Bedford estimator model (used in Figure 21) to all sixteen pilots, and it is seen that the fit remains quite high.

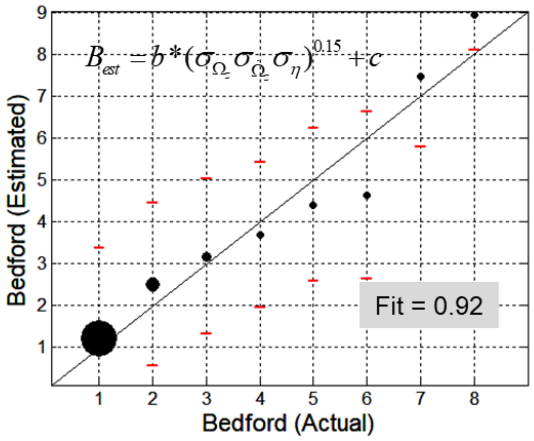

Figure 22. Bedford estimate comparison using $\Omega\dot{\Omega}\eta$ for all sixteen pilots. Black dots denote mean, red bars denote standard deviation, radius of black dots denotes relative percentage of total measurements that comprise the average.

It may be inferred from this that the variables tracked for the approach task will include one or more from Ω_z, $\dot{\Omega}_z$ and η. Producing the best fit with workload, these were selected for the Bedford estimator for the Coaxial aircraft.

Example Time History Comparisons

Figure 23 compares the Bedford estimator (magenta) with the actual Bedford ratings (blue) for four different pilots. Each of the histories ends when the aircraft meets the following criteria: less than 80 feet from the LZ, less than 20 feet above the ground, and less than 2 knots in forward speed. Agreement is generally quite good both in phase and amplitude.

Bachelder et al. [16] showed that performance is partly composed of workload, but it does not follow that the sources that drive workload are the only ones that are used for control. Correspondence with control activity is a basic first check for whether a variable may employed for controlling the task – as noted earlier, correspondence doesn't guarantee causality, but lack of correspondence will rule out causality.

To illustrate the correspondence between flow rate and stick rate, Figure 24 compares the standard deviation of the longitudinal stick rate raised to the power of 0.15, $(\sigma_{\delta_x})^{0.15}$, with $(\sigma_{\Omega_x\dot{\Omega}_x})^{0.15}$ for four

Presented at 44th European Rotorcraft Forum, Delft, The Netherlands, 18-21 September, 2018

approaches (different pilots). The exponent 0.15 was selected because it produced the best fit with the pilot ratings. Figure 25 does the same type of comparison for the vertical axis between $(\sigma_{\delta_z})^{0.15}$ (collective) $(\sigma_{\Omega_z\dot{\Omega}_z})^{0.15}$. Phase and amplitude between stick rate and the product of optic flow and optic flow rate appears to match well for both the longitudinal and vertical axes (agreement was similarly good in the lateral axis).

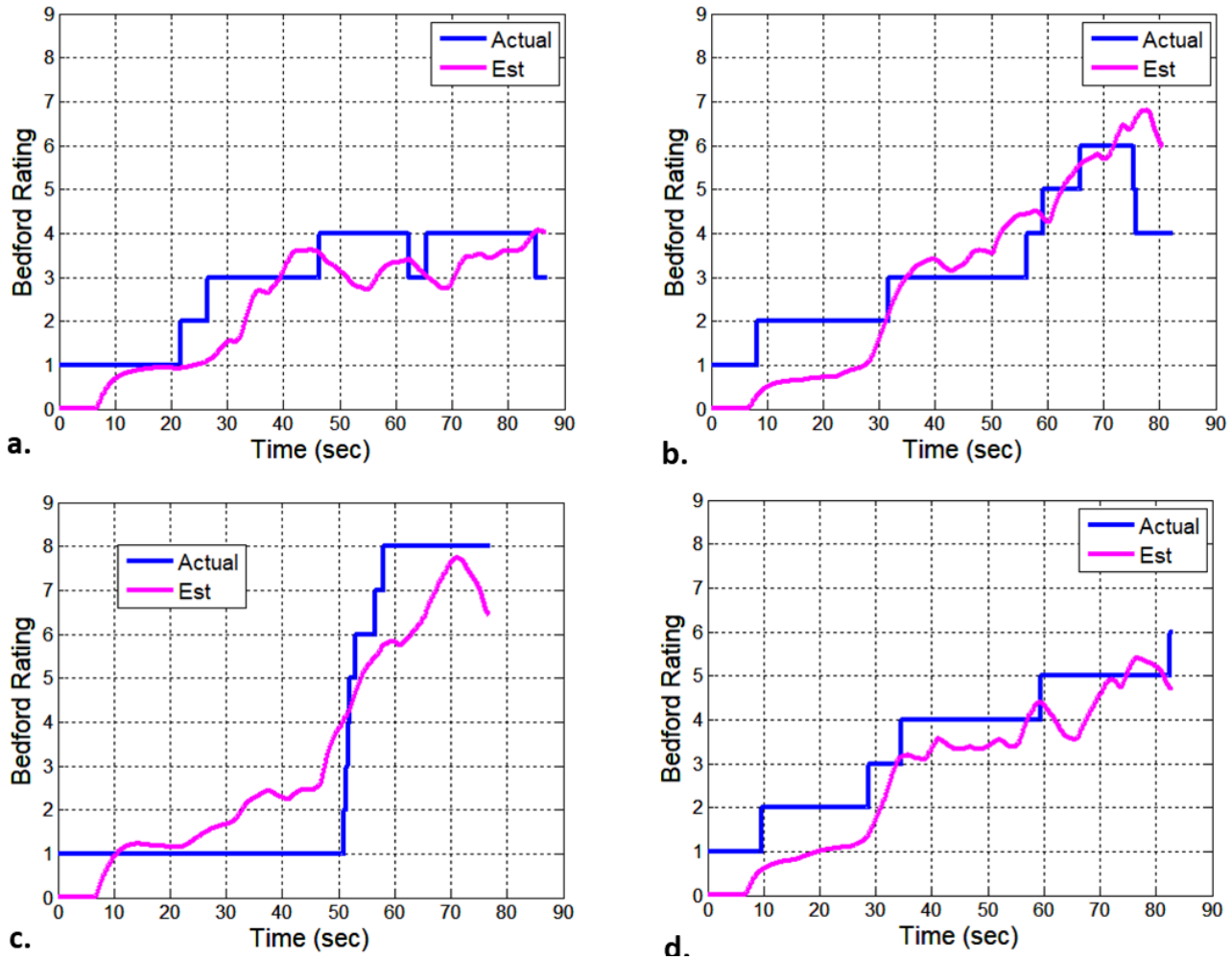

Figure 23. Bedford estimates for different pilots: a) 200' entry b) 600' entry; c) 200' entry d) 600' entry.

Presented at 44th European Rotorcraft Forum, Delft, The Netherlands, 18-21 September, 2018

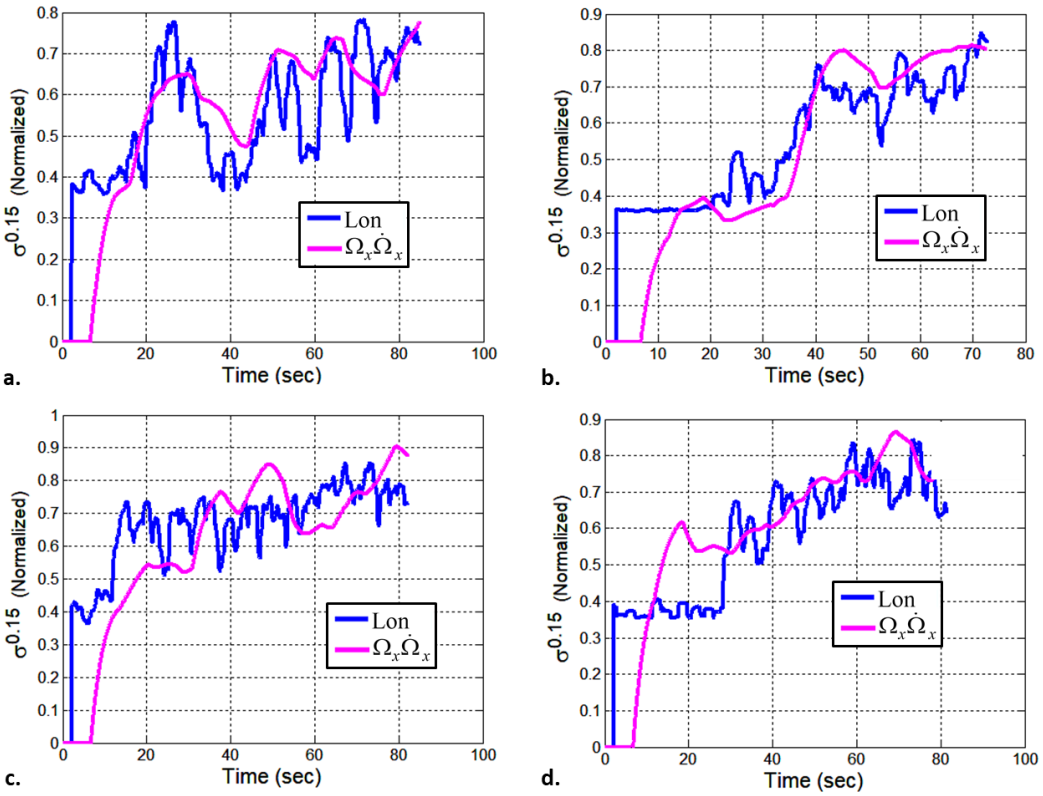

Figure 24. Longitudinal stick rate response and $\Omega_x\dot{\Omega}_x$ comparisons for different pilots: a) 600' entry b) 600' entry; c) 200' entry d) 200' entry.

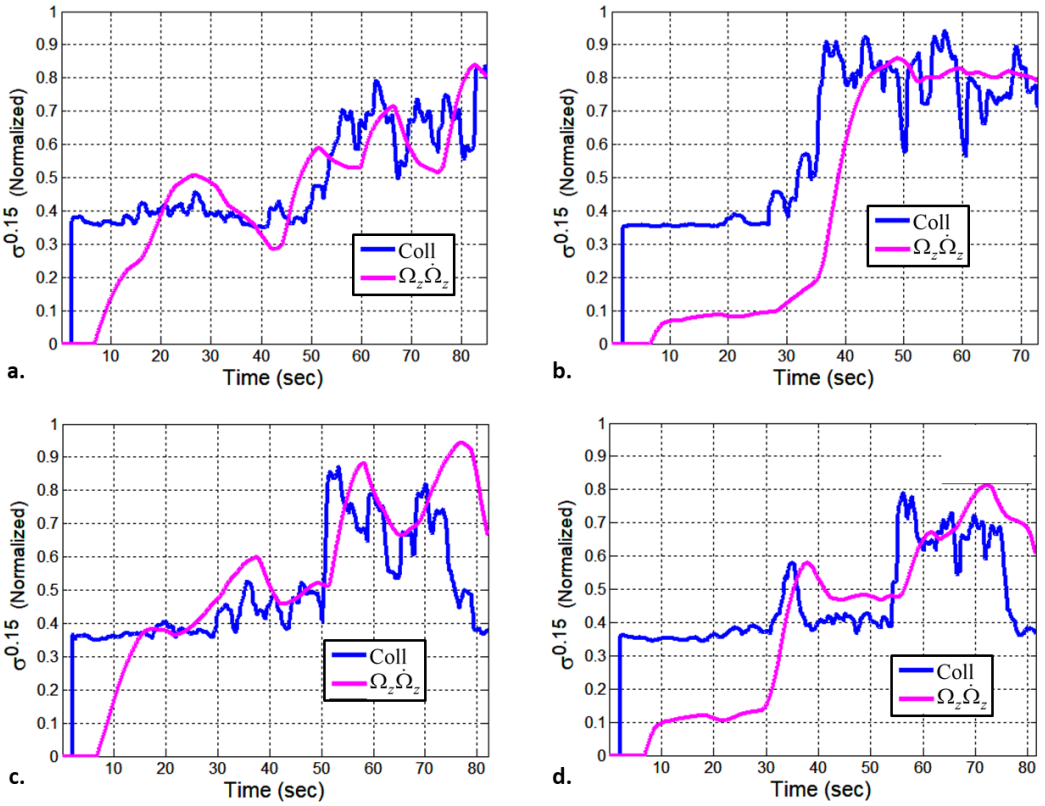

Figure 25. Collective rate response and $\Omega_z\dot{\Omega}_z$ comparisons for different pilots: a) 600' entry b) 600' entry; c) 200' entry d) 200' entry.

Presented at 44th European Rotorcraft Forum, Delft, The Netherlands, 18-21 September, 2018

Optic Flow and Constant Glidepath Angle

Figure 26 shows a typical time-history of optic flow observed in the experiment (single pilot, single trial). Approach entry occurs at 37 seconds, after which there are momentary spikes in the optic flow until the very end of the manoeuvre during the flare (around the 60-second mark). It appears the optic flow is generally constant, which is consistent with the correlation analysis which pointed to workload being strongly correlated to both Ω_z and $\dot{\Omega}_z$. Thus a candidate control strategy could be to set Ω_{tot} at entry and attempt to maintain that level of optic flow more or less constant (i.e., keep $\dot{\Omega}_{tot} \approx 0$).

For ease of presentation Figure 27 repeats Figure 3, depicting the approximate optic flow for viewing a point on a vertical plane and a horizontal plane during helicopter translation. The requirement for keeping the LZ in sight (i.e. seeing the LZ above the cockpit glareshield) guarantees small enough ς such that $\tan(\varsigma) \approx \varsigma$.

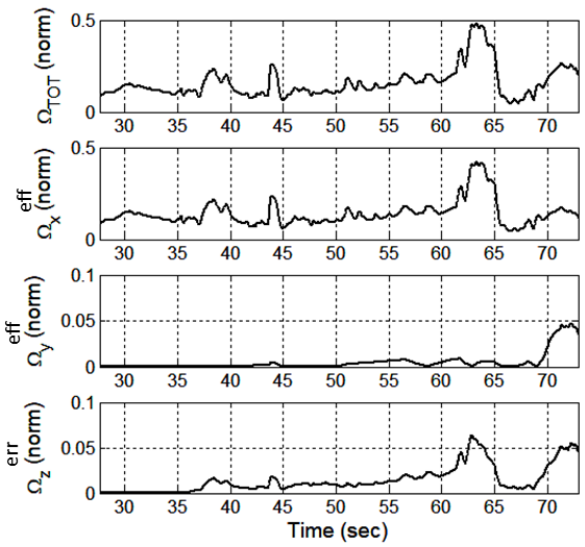

Figure 26. Normalized effective optical flow (sum of magnitudes): a) Total; b) Forward axis; c) Lateral axis; d) Vertical axis (note the different scale in c and d).

If the pilot were to fly a constant glidepath angle γ to the LZ, the instantaneous time-to-arrive (τ) would be the same for both the *x* and *z* axes of motion, since the speeds V_x and V_z are proportionally related (see Figure 28, Eqn. 21). *D* and *H* are similarly related through γ, and the vertical plane Eqn. 22 shows that the optic flow $\dot{\beta}$ is inversely related to τ. If the pilot strategy were to keep $\dot{\beta}$ constant, this would require $\dot{\tau} \approx 0$ (Eqn. 23). A similar result is obtained if the optic flow along the horizontal plane ($\dot{\varsigma}$) is kept constant in Eqn. 25. Generalizing this for all the points that may be generating perceivable optic flow in the vertical and horizontal planes, Eqn. 26 shows $\Omega_{tot} \approx$ constant.

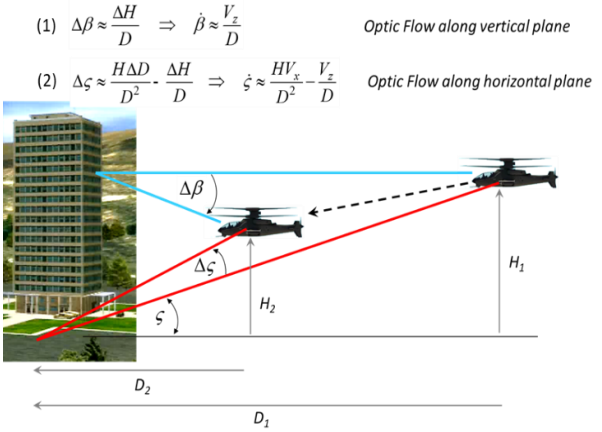

Figure 27. Optic flow for viewing a point on a vertical plane and horizontal plane during helicopter translation.

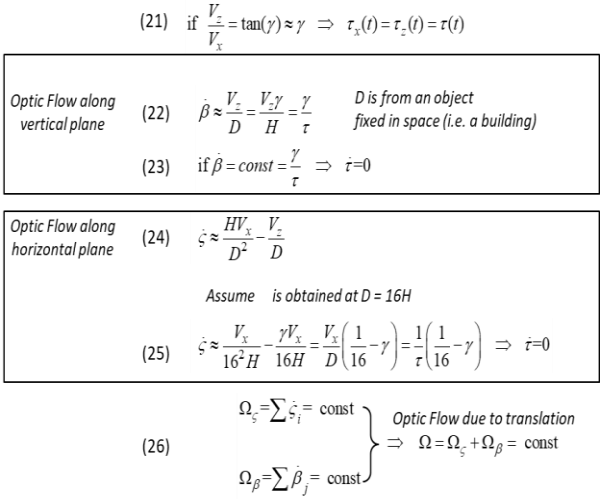

Figure 28. Relationships governing optic flow due to forward and vertical translation during a constant glidepath angle approach.

Padfield et al. [13] demonstrated that for a quick-stop manoeuvre (where the helicopter rapidly decelerates to a hover while maintaining constant altitude) pilots tend to reduce τ at a steady rate of about 0.6 (sec/sec). For another task (transitioning from level near-earth flight to flight over constant-sloped terrain) $\dot{\tau}$ was observed to be approximately 0.35 for much of the maneuver. Examining flight data from the Coaxial aircraft (two different pilots), Figure 29 shows the vertical and horizontal speed histories (blue) for two different approach condition. Two simulated trajectories are

Presented at 44th European Rotorcraft Forum, Delft, The Netherlands, 18-21 September, 2018

superimposed, one corresponding to $\dot{\tau} = 0.5$ (magenta dots), and the other to $\dot{\tau} = 0$ (cyan dots). The simulated paths begin when vertical speed has reached a maximum descent rate, using the actual forward speed as their forward entry speed. The flight path angle γ is set at the LOS angle to the LZ at the instant of entry, and the vertical speed is slaved to the horizontal speed via γ. The profiles corresponding to $\dot{\tau} = 0.5$ terminates prematurely for approaches, and their straight-line paths do not conform well to actual flight. When $\dot{\tau} = 0$, the timing and amplitude of the paths match the overall flight data quite well, despite the deep oscillations that occur in both V_x and V_z. This example serves to reinforce the hypothesis that Ω_{tot} is established at entry, and the pilot attempts to maintain that level of optic flow constant (i.e., keep $\dot{\Omega}_{tot} \approx 0$).

Stick Rate Correlation with Workload Across Aircraft

Table 8 gives the fit, mean error, and STD of the error between collective stick rate and workload, using Eqn. 19. The weak correlation between stick rate and workload in the Tilt-rotor, and weaker still correlation in the UH-60, may have been due in part to the increased motion coupling between axes for the two aircraft, compared to the Coaxial.

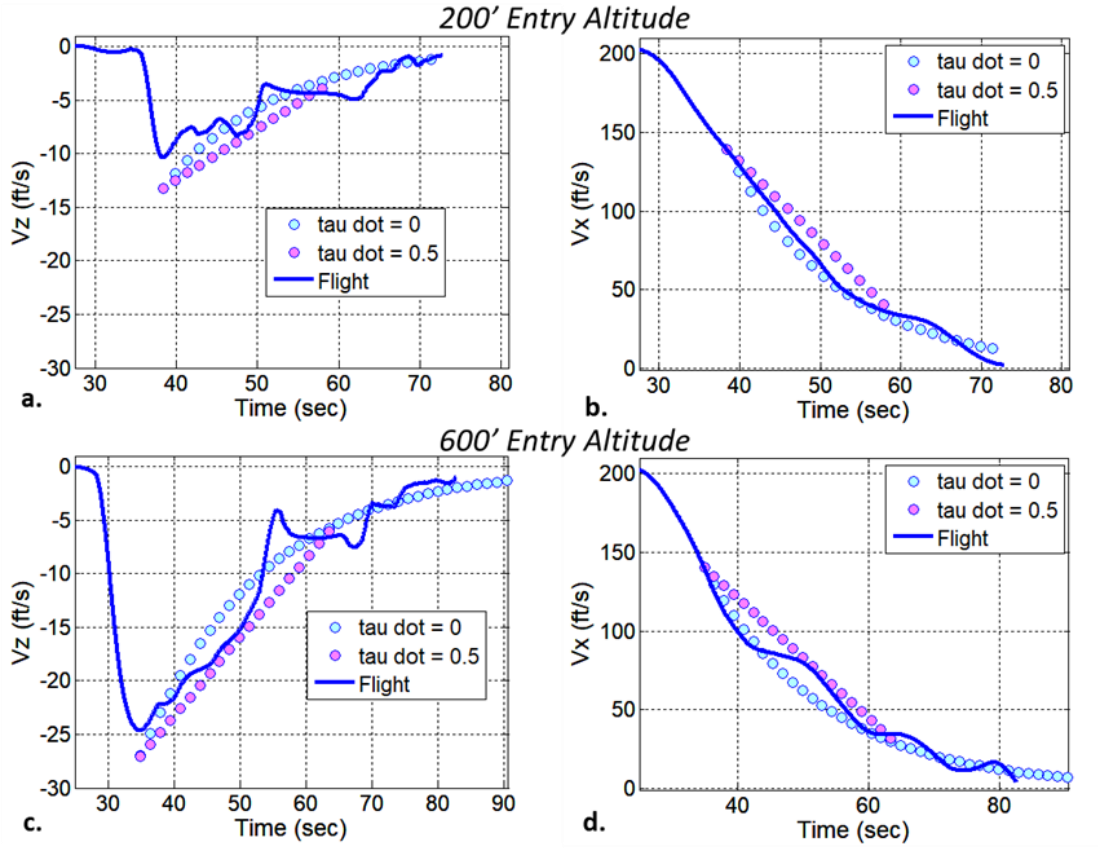

Figure 29. Simulated $\dot{\tau}$ comparisons with flight data. Top row (Pilot 1): 200 ' entry: a) Sink rate; b) Forward speed; Bottom row (Pilot 2): 600' entry: c) Sink rate; d) Forward speed. Simulation begins when maximum sink rate (flight data) is reached

Table 8. Correlation measures for collective rate and workload across aircraft.

Aircraft	Fit	Avg(B_{err})	std(B_{err})
Coaxial	0.95	0.45	1.09
Tilt-rotor	0.89	0.75	2.00
UH-60	0.79	0.93	3.74

Presented at 44th European Rotorcraft Forum, Delft, The Netherlands, 18-21 September, 2018

Investigating the Observer Effect

The process for collecting Bedford ratings during flight was designed to provide useful and timely information on workload while minimally affect the pilot's task performance. A preliminary examination of how workload collection may have influenced the pilot is shown in Figure 30. During a particular run one of the pilots was mistakenly not prompted for workload ratings, and neither did he provide Bedford updates while flying this run (performance is shown in Figure 30a). The flight subsequent to this did include the ratings, and is shown in Figure 30b. Both flights are nearly identical, and the run that collected workload was even completed a few seconds earlier than when there were no workload ratings given.

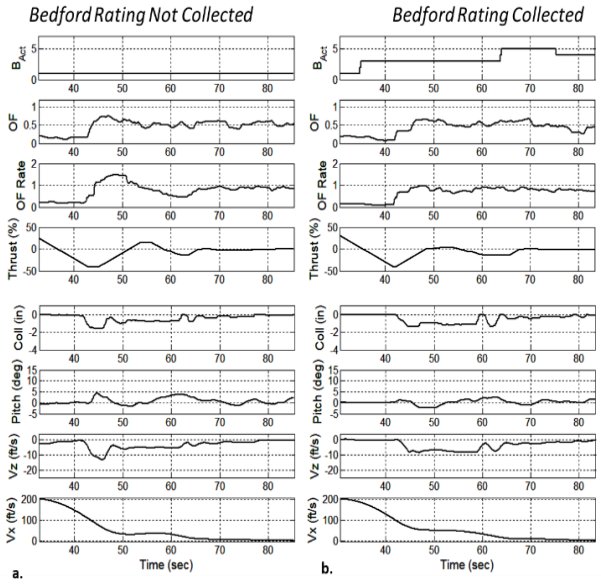

Figure 30. Comparison of approach performance: a) Bedford ratings not collected during flight; b) Bedford ratings collected throughout flight.

5.1.2 Performance Outlier

One of the pilots tested completed the approaches with times that were consistently faster than the other pilots – for all three vehicle types. His performance will be examined in detail in a future paper, but the following comparison will serve to emphasize his superlative abilities. Using the actual model's dynamics, an optimal solution for minimum-time landing in the coaxial aircraft was generated and is shown in Figure 31a. The entry altitude was 600 feet. Figure 31b plots the "Golden Arm" pilot's control profiles for the same approach. The similitude of the two responses in thrust, collective, and pitch are striking, but what is perhaps most notable is that the pilot arrived to the LZ *faster* than the optimal solution.

An interesting difference in background between this pilot and the other test subject is the aircraft he flies at his unit – the UH-1Y "Super Huey". This is a four-bladed medium-sized utility helicopter which, unlike the larger vehicles flown by the other pilots, can be flown to touchdown when practicing autorotations. Autorotation is the term for power-off flight where the air stream enters the main rotors from below rather than above, as occurs during powered flight. This manoeuvre is often practiced by military helicopter pilots, but due to the cost and sensitivity of onboard avionics associated with heavier helicopters the practice autorotation must be terminated prior to touchdown and powered flight resumed. It is in the final fifty feet of a 'full' autorotation (to the ground) that the so-called 'ground rush' (optical flow) reaches a maximum, and considerable practice is required to recognize and control the trade-offs between ground rush and energy dissipation. All military helicopter pilots learn to fly full autorotations in their primary flight training with lighter platforms, but barring an actual engine failure most never fly another full 'auto' once they leave their training command.

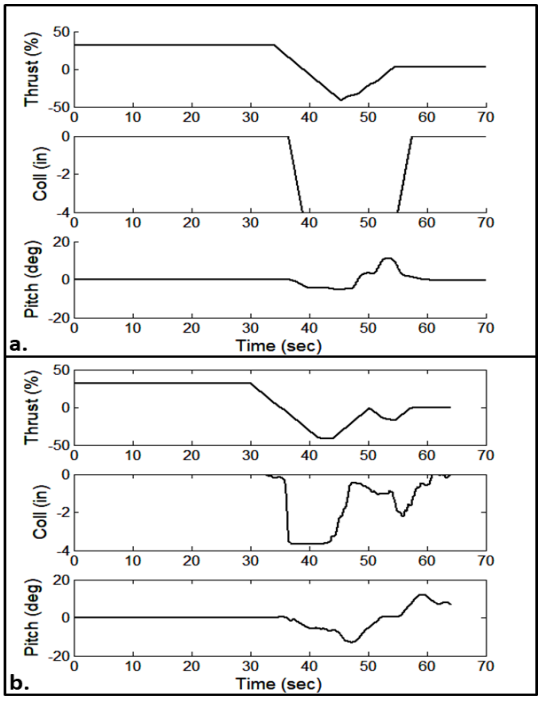

Figure 31. Control profiles for minimum-time 600' entry approach (coaxial aircraft): a) Computer-generated optimal solution; b) "Golden Arm" pilot.

The Golden Arm pilot would have had continuous exposure to full autorotations, and thus may have had increased sensitivity to changes in optic flow and been able to anticipate control inputs needed to maintain tight trajectory control – even in the presence of uncertain aircraft dynamics. In a related area, autonomous power-off flight has been a topic of interest for the last several decades, and

Presented at 44th European Rotorcraft Forum, Delft, The Netherlands, 18-21 September, 2018

control of optic flow may be an effective, robust approach for autonomously executing of autorotations.

6. SUMMARY

A simulation experiment was conducted to evaluate the workload associated with operating a compound (coaxial-rotor and push-prop) vehicle model, a tilt-rotor vehicle model, and a UH-60 model. Sixteen experienced military pilots flew aggressive visual approaches terminating in a hover while providing Bedford workload ratings in real time. Prior work identified a mathematical relationship between pilot workload and the combination of display error rate and stick rate during compensatory tracking tasks. The current work extends this relationship to visual landing approaches, where the pilot is hypothesized to track key optical variables that are available from the OTW scene. Via correlation analysis a set of candidate tracking variables which appears to drive pilot workload is identified: optic flow, and the angle formed between the cockpit glareshield and the intended landing spot. Combined with stick rate these variables are used to generate a Bedford estimate. Actual and modeled Bedford ratings were compared for the Coaxial aircraft. Innovative contributions of this research include: 1) Optical flow from high resolution, high frame rate flight video is computed and analyzed for workload analysis; 2) A modelling technique is developed that produces workload estimates that closely matches actual pilot ratings; 3) A technique based on visual perceptual requirements allows optical flow to be employed in a very simplistic, tractable, yet effective manner; 4) While tau motion theory (i.e. rate of instantaneous time-to-arrive is approximately constant) was roughly observed during the approaches, it appears that tau motion was a result of the pilot adhering to a strategy of minimizing deviation in optic flow rather than being the source of pilot behavior; 5) Using a novel method, Bedford workload ratings were collected in real time without impinging on the flight task, enabling in-situ workload analysis.

The following summarizes the findings related to optic flow (Coaxial aircraft)

- Optic flow (Ω) was generally observed to stay constant throughout the approach, and changes in Ω and its rate $\dot{\Omega}$ correlated strongly with changes in workload.
- Optic flow (Ω) associated with vertical motion affected workload the most.
- The observed aircraft trajectories exhibited approximately constant tau (τ) (overall), reinforcing the hypothesis that as a control strategy Ω is established at entry. Subsequently the pilot attempts to maintain that level of optic flow constant (i.e., keep $\dot{\Omega} \approx 0$). This is consistent with Army training instruction.
- In the short-term, tau was significantly oscillatory for the longitudinal axis, and most often erratic with large amplitude excursions in the vertical axis. Correlation of tau with workload was poor for both axes, indicating tau was not a primary influence on control or workload.
- The phase and amplitude of stick rate, and the product of Ω and $\dot{\Omega}$ appears to match well in all axes, further suggesting that the pilot may be tracking these two variables as a control strategy.
- The set of variables that produced the best fit with workload was $\dot{\delta}_z$, Ω_z, and η, and these were used for the Bedford estimator employing the Power Law producing an excellent fit.

7. FUTURE WORK

The workload model developed using the coaxial aircraft optic flow analysis will be applied using the tilt-rotor and Blackhawk aircraft optic flow in the future when that data is computed.

Autonomous power-off flight has been a topic of interest for the last several decades, and control of optic flow may be an effective, robust approach for autonomously executing autorotations.

An area of focused research in Army Aviation is Optionally Piloted Vehicle (OPV) flight. If a pilot has transferred control to automation during an approach, pilot trust may be higher if he/she observes system behavior that resembles what a skilled operator would produce. This not only applies to the motion of inceptors (cyclic, collective, pedals), but also the visual cues that the commanded flight trajectory generates. Identifying what visual cue set is used by pilots, and how the cues are controlled, would allow an automated system to emulate pilot strategy and produce an OTW response familiar to the pilot. This study indicates that an outcome of adhering to a pilot strategy of optical flow control during an aggressive visual approach could be reduced workload. This hypothesis will be evaluated in future OPV testing.

Acknowledgments

Steve Norris, Senior Simulation Engineer of the VMS facility, painstakingly customized and tested the various elements required for this experiment

Presented at 44th European Rotorcraft Forum, Delft, The Netherlands, 18-21 September, 2018

to ‘piggy-back’ on the over-arching Operations Concept Team experiment. Terry Turpin of ADD Ames assisted in construction and testing of the experimental design, the running of participants, and gave key insight to Army instructor technique. Major Zachariah Morford flew the design as a pre-test subject, providing data and comments that were critical to the project’s success. Major Jonathan Mulder proposed a novel hypothesis linking the Golden Arm pilot’s superior performance and his operational experience. A debt of gratitude is owed to the pilots who devoted their time, interest, and skill participating in the testing evolution. This work was supported by cooperative agreement NNX16AJ91A between the U.S. Army Aviation Development Directorate and San Jose State University. This paper has been approved for public release: unlimited distribution.

Biographies

Dr. Edward Bachelder is a senior Research Engineer at ADD, Moffett Field, CA. He flew the SH-60B Seahawk as a Naval Aviator prior to his doctoral research at MIT. His current research includes modelling pilot control and workload, and advanced display design.

Dr. Martine Godfroy-Cooper is a senior Research Psychologist at NASA ARC, CA. Her research interests encompass multisensory integration, advanced controls and displays and perception-action coupling.

Mr. Bimal Aponso Bimal Aponso is the Associate Chief for Aeronautics in the Intelligent Systems Division at NAS Ames Research Center. Bimal's technical background includes over 25-years of experience in vehicle modelling and simulation, stability and control, and handling qualities, both in government and in Industry. He researched, designed and developed flight control systems for several military and civil aircraft and rotorcraft, and contributed to several Military Specifications on aircraft/rotorcraft handling qualities.

Mr. Chris Blanken began working for the U.S. Army's Aviation Development Directorate in 1980, where he's now the lead for the Vehicle Management and Control Technical Area. Chris was the Army project engineer for the development of the Aeronautical Design Standard–33 (ADS-33E-PRF), a military rotorcraft handling qualities performance specification.

Mr. Tom Berger is a Research Aerospace Engineer with the US Army Aviation Development Directorate at Moffett Field, California. He specializes in fixed- and rotary-wing aircraft system identification, flight control design, and handling qualities.

Appendix A

Bedford Scale

The Bedford rating scale is a three-rank ordinal structure used to assess pilot workload defined as: “… the integrated mental and physical effort required to satisfy the perceived demands of a specified flight task” (Roscoe, 1984). The concept of spare capacity is used to help define levels of workload.

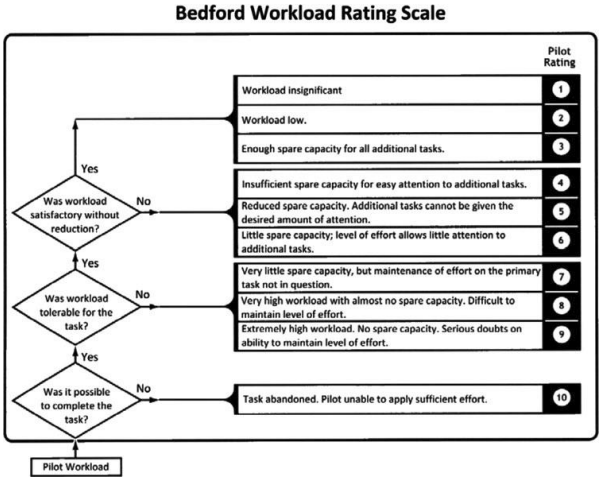

References

[1] Andrew Burton & John Radford (1978). Thinking in Perspective: Critical Essays in the Study of Thought Processes. Routledge. ISBN 0-416-85840-6.

[2] David H. Warren & Edward R. Strelow (1985). Electronic Spatial Sensing for the Blind: Contributions from Perception. Springer. ISBN 90-247-2689-1.

[3] Gibson, J.J. (1950). The Perception of the Visual World. Houghton Mifflin.

[4] http://vision.middlebury.edu/flow/

[5] Andrés BruhnJoachim WeickertChristoph Schnörr, Lucas/Kanade Meets Horn/Schunck: Combining Local and Global Optic Flow Methods, International Journal of Computer Vision, February 2005, Volume 61, Issue 3, pp 211–231.

[6] BKP Horn, BG Schunck, Determining Optical Flow, Artificial intelligence, 1981 – Elsevier.

[7] J. Barraza, N. Grzywacz, “Parametric decomposition of optic flow by humans”, Vision Research, 2005 Sep;45(19):2481-91.

[8] M Lappe, F Bremmer, AV Van den Berg, Perception of self-motion from visual flow, Trends in cognitive sciences, 1999 – Elsevier.

[9] Jack M. Loomis & Andrew C. Beall, Visually Controlled Locomotion: Its Dependence on Optic Flow, Three-

Dimensional Space Perception, and Cognition, Pages 271-285 | Published online: 22 Jun 2011.

[10] Lee, D. N. (1976). A theory of visual control of braking based on information about time-to-collision Perception, 5,437-459.

[11] Yilnaz, E. H., &Warren, W. H. (1995). Visual control of braking: A test of th tau-dot hypothesis.]~~ MI of Experimental Psychology: Human Perception and Performance, 21,99 1014.

[12] Flach, J. M., Stanard, T., &Smith, M. R. H. (in press). Perception and control of collisions: An altema. tive to the tau hypothesis. InM. McBeath (Ed.), Spatialnavigatid~ipksutedby humnns,animals, and machines. Thousand Oaks, CA: Sage.

[13] G. Padfield, G. Clark, A. Taghizad, How Long Do Pilots Look Forward? Prospective Visual Guidance in Terrain-Hugging Flight, Journal of the American Helicopter Society, Volume 52, Number 2, 1 April 2007, pp. 134-145(12).

[14] Tustin, A., "The nature of the human operators response in manual control and its implication for controller design," J. Instn. Elect. Engrs, 94, 190, 1947.

[15] McRuer, D. T. and Krendel, E. S., "Mathematical Models of Human Pilot Behavior," No. AGARDograph No. 188, November 1973.

[16] E. Bachelder, R. Hess, M. Godfroy-Cooper, B. Aponso, "Linking the Pilot Structural Model and Pilot Workload", 2018 AIAA Atmospheric Flight Mechanics Conference, 0533.

[17] Hess, R. A., "Unified Theory for Aircraft Handling Qualities and Adverse Aircraft-Pilot Coupling", Journal of Guidance, Control, and Dynamics, Vol. 20, No. 6, 1997.

[18] Hess, R. A., "Pursuit Tracking and Higher Levels of Skill Development in the Human Pilot", IEEE Transactions on Systems, Man, and Cybernetics, Volume: 11, Issue: 4, April 1981.

[19] Edward Bachelder, Bimal Aponso, Martine Godfroy, "Characterization of Pilot Technique", 73rd Annual American Helicopter Society Forum & Technology Display; 9-11 May 2017; Fort Worth, TX.

[20] Linghai Lu, Michael Jump, and Gareth D. Padfield. "Development of a Generic Time-to-Contact Pilot Guidance Model", Journal of Guidance, Control, and Dynamics, Vol. 41, No. 4 (2018), pp. 904-915.

https://doi.org/10.2514/1.G003135

[21] Golnaraghi, F., and Kuo, B., Automatic Control Systems, WileyBlackwell, Hoboken, NJ, 2003.

[22] Juhasz, O., Celi, R., Ivler, C. M., Tischler, M. B., and Berger, T., "Flight Dynamic Simulation Modeling of Large Flexible Tiltrotor Aircraft," presented at the American Helicopter Society 68th Annual, May 2012, Fort Worth, TX.

[23] Celi, R., "HeliUM 2 Flight Dynamic Simulation Model: Developments, Technical Concepts, and Applications," presented at the American Helicopter Society 71st Annual Forum, May 2015, Virginia Beach, VA.

[24] Johnson, W., Moodie, A. M., and Yeo, H., "Design and Performance of Lift-Offset Rotorcraft for Short-Haul Missions," presented at the American Helicopter Society Future Vertical Lift Aircraft Design Conference, January 2012, San Francisco, CA.

[25] Berger, T., Juhasz, O., Tischler, M. B., and Horn, J. F.," Modeling and Control of Lift Offset Coaxial and Tiltrotor Rotorcraft," presented at the 44th European Rotorcraft Forum, September 2018, Delft, The Netherlands.

[26] E. Bachelder, M. Godfroy, Pilot Workload Estimation: Synthesis of Spectral Requirements Analysis and Weber's Law, 2019 AIAA Modeling and Simulation Conference (in press).

Presented at 44th European Rotorcraft Forum, Delft, The Netherlands, 18-21 September, 2018